PAPER • OPEN ACCESS

Structures and Lagrangian statistics of the Taylor–Green dynamo

New Journal of Physics
The open access journal at the forefront of physics
Deutsche Physikalische Gesellschaft DPG | IOP Institute of Physics

Structures and Lagrangian statistics of the Taylor–Green dynamo

H Homann[1], Y Ponty[1], G Krstulovic[1] and R Grauer[2]
[1] Université de Nice-Sophia, CNRS, Observatoire de la Côte d'Azur, CS 34229, F-06304 Nice Cedex 4, France
[2] Institut für Theoretische Physik I, Ruhr-Universität Bochum, D-44780 Bochum, Germany
E-mail: holger.homann@oca.eu

Received 23 January 2014, revised 24 May 2014
Accepted for publication 2 June 2014
Published 24 July 2014
New Journal of Physics **16** (2014) 075014
doi:10.1088/1367-2630/16/7/075014

Abstract
The evolution of a Taylor–Green forced magnetohydrodynamic system showing dynamo activity is analyzed via direct numerical simulations. The statistical properties of the velocity and magnetic fields in Eulerian and Lagrangian coordinates are found to change between the kinematic, nonlinear and saturated regime. Fluid element (tracer) trajectories change from chaotic quasi-isotropic (kinematic phase) to mean magnetic field aligned (saturated phase). The probability density functions (PDFs) of the magnetic field change from strongly non-Gaussian in the kinematic to quasi-Gaussian PDFs in the saturated regime so that their flatness give a precise handle on the definition of the limiting points of the three regimes. Also the statistics of the kinetic and magnetic fluctuations along fluid trajectories changes. All this goes along with a dramatic increase of the correlation time of the velocity and magnetic fields experienced by tracers, significantly exceeding one turbulent large-eddy turn-over time. A remarkable consequence is an intermittent scaling regime of the Lagrangian magnetic field structure functions at unusually long time scales.

S Online supplementary data available from stacks.iop.org/njp/16/075014/mmedia

Keywords: MHD turbulence, Lagrangian statistics, Taylor–Green flow, magnetic dynamo

1. introduction

The magnetic field of stars and telluric planets is explained by the dynamo instability, produced by a turbulent conducting fluid where the induction due to the motion takes over the magnetic diffusion. A system with dynamo action passes through different stages from the linear (kinematic) to the nonlinear and finally to the saturated phase. During the kinematic phase the magnetic energy grows exponentially but has no influence on the flow. During the nonlinear phase the Lorentz force changes the flow and at the saturation state the diffusion and the electromotive force reach equilibrium. The system reaches the fully nonlinear magnetohydrodynamic (MHD) regime, driven by an energy exchange between the velocity and magnetic field.

In the last decade, several experimental groups have investigated dynamo action in laboratory experiments using liquid sodium [1–3]. The instability threshold and a rich nonlinear behavior along the saturation regime have been largely observed [4–6]. Investigations of the fast kinematic dynamo [7] in the 1990s, showed the important role of the chaotic properties of the fluid trajectories for the dynamo threshold. The effect of turbulent fluctuations on the dynamo onset has also been studied in Navier–Stokes flows [8, 9] and some noisy models [10], distinguishing the important role between the mean flow dynamo and fluctuation dynamo modes [11].

The transition between the linear and the saturation regime has been studied measuring the finite-time Lyapunov exponent of the flow trajectories [12, 13]. These results showed a strong reduction of the chaotic properties in the saturation phase, due to the action of the Lorentz force. Fluid trajectories thus change along the different dynamo phases. This naturally motivates the use of a Lagrangian description where the properties of the flow are investigated by using tracers [14].

Lagrangian statistics describes the dynamical evolution of physical quantities along tracer trajectories in contrast to the Eulerian perspective in which such quantities are analyzed on fixed spatial points. During recent decades, Lagrangian studies have revealed new aspects of homogeneous and isotropic turbulence [15]. The trajectory point of view has shown to be especially useful for the study of coherent structures and intermittency [16–18] as well as for diffusion and dispersion properties of hydrodynamic and MHD turbulence [19–21]. This approach has produced many experimental results by tracking solid inertial particles or bubbles [22, 23], which can have a different dynamics compared to simple tracers. Lagrangian statistics has also been used in MHD simulations [24, 25] to compare the anomalous exponents of the structure function to their hydrodynamic counterparts and to understand the relation between Eulerian and Lagrangian statistics. In the Kraichnan–Kazantsev framework the latter was used to determine the dynamo onset as a function of the roughness of the flow [26].

The aim of this work is to use standard tools of Lagrangian turbulence in the context of turbulent MHD dynamos. This approach highlights new aspects of dynamo action. For instance it shows that magnetic field fluctuations along fluid trajectories are intermittent and allows to precisely define the limiting points of different dynamo regimes. Furthermore, the Lagrangian perspective evidences a strong correlation of the mean magnetic field structures and the fluid

trajectories which is connected to our knowledge unknown scaling regime at time scales well beyond usual turbulent scales.

The dynamo systems under consideration in this work is induced mainly by the so-called Taylor–Green (TG) forcing [27]. For comparison, a second forcing where the large scales of the velocity field are frozen in time is also considered. The TG flow, which can produce dynamo action, is a very well documented study case involving rich dynamo behaviors in both the linear and the nonlinear regime [8, 10, 28–32]. The TG flow contained in a periodic box has several properties that mimic the von Kàrmàn flow, driven by two counter-rotating impellers. The von Kàrmàn flow has a strong experimental history inside the turbulent and the dynamo scientific communities. Indeed, several teams set up such experiments with different designs in water [33, 37] and air flows [34–36]. This type of experiment was also one of the first setups used to study Lagrangian statistics of turbulent flows [22, 23]. After the intensive water campaign experiments of the Saclay group [38, 39], this setup has lead to the von Kàrmàn sodium (VKS) dynamo campaigns also cited above.

This paper is organized as follows: in the next section the dynamo system under consideration and the numerical method are explained. In section 3, the evolution of the flow structure and trajectories within the three different regimes are discussed. Section 4 investigates the changes of the velocity and magnetic field fluctuations from one regime to another from the Eulerian point. In section 5, Lagrangian statistics are presented and, amongst other results, a magnetic field scaling regime at very large temporal scales is reported. Conclusions are drawn in section 6.

2. Model and methods

We perform direct numerical simulations of turbulent MHD flows with large-scale forcing in a periodic cube. We integrate the three-dimensional incompressible MHD equations that, expressed in Alfvénic units, read

$$\partial_t \boldsymbol{u} + \boldsymbol{u} \cdot \nabla \boldsymbol{u} = (\nabla \times \boldsymbol{B}) \times \boldsymbol{B} - \nabla p + \nu \nabla^2 \boldsymbol{u} + \boldsymbol{F}, \tag{1}$$

$$\partial_t \boldsymbol{B} = \nabla \times (\boldsymbol{u} \times \boldsymbol{B}) + \eta \nabla^2 \boldsymbol{B}, \tag{2}$$

$$\nabla \cdot \boldsymbol{u} = 0, \quad \nabla \cdot \boldsymbol{B} = 0, \tag{3}$$

where ν and η are the kinematic viscosity and the magnetic diffusivity respectively. The density of the fluid is set to unity and $\boldsymbol{F}$ is the constant volume force which generates and maintains the turbulent flow. For most simulations (see table 1) we consider the so called TG flow that is generated by forcing with the TG vortex

$$\boldsymbol{F}_{\mathrm{TG}} = F_0 \big(\sin(k_0 x) \cos(k_0 y) \cos(k_0 z) , - \cos(k_0 x) \sin(k_0 y) \cos(k_0 z), \ 0\big), \tag{4}$$

with $F_0 = 3$ and $k_0 = 1$ or $k_0 = 2$. When $k_0 = 1$, this forcing leads to a subdivision of the total domain in eight fundamental cubes (each of the same size) that, when symmetries are preserved, can be related to each other by mirror-symmetric transformations. Each fundamental box contains a swirling flow composed of a shear layer between two counter-rotating eddies. It is this flow structure which relates to the von Kàrmàn flow. As we will see in the following sections, the TG dynamo action presents some particular properties due to its anisotropy. In order to distinguish universal and non-universal properties of the TG dynamo action we also

Table 1. List of the numerical simulations. $Pm = \nu/\eta$: magnetic Prandtl number, $Re = u^{\mathrm{rms}}\, L/\nu$: Reynolds number, u^{rms} root mean square velocity (defined in table 2), $\left(Rm - Rm_c\right)/Rm_c$: bifurcation parameter where Rm_c is the critical magnetic Reynolds number, N number of collocation points, N_p number of tracer particles.

Run	Regime	Pm	Re	$\left(Rm - Rm_c\right)/Rm_c$	Force type	N	N_p
tgH	Hydro	—	350	—	TG ($k_0 = 1$)	256^3	2×10^5
tg1	Saturated	1/4	297	0.11	TG ($k_0 = 1$)	256^3	2×10^5
tg2	Saturated	1/2	670	1.2	TG ($k_0 = 1$)	256^3	2×10^5
tg3	Saturated	1	676	3.5	TG ($k_0 = 1$)	256^3	2×10^5
tg4	Saturated	1	128		TG ($k_0 = 2$)	256^3	2×10^5
tg5	Saturated	1	545	2.8	TG ($k_0 = 1$)	128^3	2×10^4
ffH	Hydro	—	476	—	FF (frozen)	256^3	2×10^5
ff	Saturated	1	625	2.2	FF (frozen)	256^3	2×10^5

consider a mechanical force F (see run ffH and ff in tables 1 and 2) obtained by keeping constant all Fourier modes of the velocity field in the two lowest shells (henceforth called frozen force simulation (FF)). The values of these Fourier modes were obtained from an initially freely decaying HD simulation with a random initial seed at large scales after the flow had developed a turbulent cascade. This force is much less structured than the TG forcing and the corresponding flow is found to be nearly isotropic.

We use classical global quantities to characterize the different dynamo phases. The kinetic energy E_{kin}, the magnetic energy E_{mag}, the enstrophy Ω, the cross helicity H_C, and the magnetic helicity H_M are defined as

$$E_{\mathrm{kin}} = \frac{1}{2}\left\langle \mathbf{u}^2 \right\rangle, \quad E_{\mathrm{mag}} = \frac{1}{2}\left\langle \mathbf{B}^2 \right\rangle, \quad \Omega = \frac{1}{2}\left\langle (\nabla \times \boldsymbol{u})^2 \right\rangle,$$
$$H_C = < \mathbf{u} \cdot \mathbf{B} >, \quad H_M = < \mathbf{A} \cdot \mathbf{B} >,$$

where $\langle\rangle$ stands for spatial average and $\mathbf{B} = \nabla \times \mathbf{A}$ with $\mathbf{A}$ the magnetic potential. In the ideal case ($\nu = \eta = 0$) and without forcing ($\mathbf{F} = 0$), $E_{\mathrm{tot}} = E_{\mathrm{kin}} + E_{\mathrm{mag}}$, H_C and H_M are conserved by the MHD equations.

The TG forcing (4) is purely horizontal, leading to anisotropy in both the hydrodynamic and the MHD regime. In order to quantify this anisotropy we compute the root mean square (rms) values of the perpendicular (xy-plane) and parallel (z) components of the velocity fields and define the global isotropy coefficient ρ_u^{iso} as

$$u_\perp^{\mathrm{rms}} = \left[\left\langle u_x^2 + u_y^2 \right\rangle / 2 \right]^{1/2}, \quad u_\parallel^{\mathrm{rms}} = \left\langle u_z^2 \right\rangle^{1/2},$$
$$\rho_u^{\mathrm{iso}} = u_\parallel^{\mathrm{rms}} / u_\perp^{\mathrm{rms}}, \quad \rho_B^{\mathrm{iso}} = B_\parallel^{\mathrm{rms}} / B_\perp^{\mathrm{rms}}.$$

With these definitions the average rms velocity is $u^{\mathrm{rms}} = \left[\left(2\, (u_\perp^{\mathrm{rms}})^2 + (u_\parallel^{\mathrm{rms}})^2 \right)/3 \right]^{1/2}$. We use analog definitions for the magnetic field.

There are also three important dimensionless numbers, namely the kinematic Reynolds number Re, the magnetic Reynolds number Rm and the magnetic Prandtl number Pm defined as

Table 2. Parameters of the numerical simulations. $\epsilon_{\rm k} = 2\nu \left\langle (\nabla \times \boldsymbol{u})^2 \right\rangle$: mean kinetic energy dissipation rate, $\rho_u^{iso} = u_\parallel^{\rm rms}/u_\perp^{\rm rms}$ isotropy coefficient, $l_K = \left(\nu^3/\epsilon_{\rm k}\right)^{1/4}$: Kolmogorov dissipation length scale, ν: kinematic viscosity, $\tau_K = \left(\nu/\epsilon_{\rm k}\right)^{1/2}$: Kolmogorov time scale, $L = \left(u^{\rm rms}\right)^3/\epsilon_{\rm k}$: integral scale, $T_L = L/u^{\rm rms}$: large-eddy turnover time. For all runs: size of domain = 2π. For run ffH and ff only the mean rms value of the three components $u_\perp^{\rm rms} = u_\parallel^{\rm rms} = u^{\rm rms}$ is listed which differ by less than 10%.

Run	$u_\perp^{\rm rms}$	$u_\parallel^{\rm rms}$	$B_\perp^{\rm rms}$	$B_\parallel^{\rm rms}$	$\epsilon_{\rm k}$	$\rho_u^{\rm iso}$	$\rho_B^{\rm iso}$	l_K	ν	τ_K	L	T_L
tgH	1.74	1.28	—	—	2.26	0.74	—	0.022	0.008	0.060	1.76	1.11
tg1	1.50	0.56	1.86	0.44	1.08	0.37	0.24	0.027	0.008	0.092	1.88	1.49
tg2	1.78	0.63	1.78	0.52	0.94	0.35	0.29	0.027	0.008	0.092	3.58	2.39
tg3	1.87	0.65	1.64	0.56	1.13	0.35	0.34	0.026	0.008	0.086	3.43	2.19
tg4	1.09	0.43	1.04	0.33	0.71	0.39	0.31	0.029	0.008	0.107	1.11	1.2
tg5	1.92	0.63	1.76	0.54	1.23	0.33	0.31	0.03	0.01	0.092	3.38	2.11
ffH	0.14	—	—	—	1.48×10^{-3}	≈1	≈1	0.0195	0.0006	0.64	2.0	13.8
ff	0.13	—	0.066	—	6.4×10^{-4}	≈1	≈1	0.0243	0.0006	0.99	3.05	24.4

$$Re = \frac{L\, u^{\mathrm{rms}}}{\nu}, \quad Rm = \frac{L\, u^{\mathrm{rms}}}{\eta}, \quad Pm = \frac{Rm}{Re} = \frac{\nu}{\eta}. \tag{5}$$

A useful quantity that measures the alignment of velocity and magnetic fields is the normalized cross helicity defined as $h_C = \cos[\mathbf{u}, \mathbf{B}] = H_C/\left(u^{\mathrm{rms}}\, B^{\mathrm{rms}}\right)$.

Numerical integration of the MHD equations (1)–(3) is carried out by using a fully MPI-parallel pseudo-spectral code (LaTu [24]) with a strongly stable third order Runge–Kutta temporal scheme. De-aliasing is performed using the standard 2/3 rule.

In this work we study Lagrangian aspects of dynamo action. Lagrangian statistics are obtained by tracers obeying the equations

$$\dot{\boldsymbol{X}}(\boldsymbol{x}, t) = \boldsymbol{v}(t), \quad \boldsymbol{v}(t) = \boldsymbol{u}(\boldsymbol{X}(\boldsymbol{x}, t)), \tag{6}$$

where $\boldsymbol{X}(\boldsymbol{x}, t)$ and $\boldsymbol{v}(t)$ are the position and velocity of a tracer which started at $\boldsymbol{x}$ for $t = 0$. The magnetic field along a tracer path is denoted by $\boldsymbol{b}(t) = \boldsymbol{B}(\boldsymbol{X}(\boldsymbol{x}, t))$. Note that we consider electrically neutral particles as we focus on the properties of the flow. The study of charged material particles, that induce currents and additional interactions, is left for a future study.

The values of the velocity fields and other physical quantities at the particle positions are evaluated and stored using a tricubic interpolation which is numerically efficient and accurate [40]. The equation (6) is integrated with the same third order Runge–Kutta scheme as the equation (1) for the velocity and magnetic fields. Statistical data is obtained from a large number of tracer trajectories varying from 2×10^4 to 2×10^6. A detailed list of the physical parameters for the different runs is presented in table 2.

3. Structures and trajectories

During dynamo action three phases are clearly distinguished. The linear phase, where a seed of magnetic field grows exponentially by the dynamo instability without back-reaction on the velocity field. The second stage, called the nonlinear phase, corresponds to the one where the Lorentz force starts to act on the flow and the kinetic energy slightly drops due to the transfer of kinetic energy to the magnetic field. Finally the full MHD system reaches a statistically stationary state, refereed to as the saturation regime. In figure 1 (left) the kinetic and magnetic energy is displayed for the TG flow. The three phases of dynamo action are separated by dashed vertical lines. In figure 1 (right) the enstrophy Ω is shown for the same simulation. When the magnetic energy attains a magnitude of the order of one percent of the kinetic energy the enstrophy drops. A comparison of different simulations shows that the vorticity drop increases when decreasing Pm (or Rm) (not shown). Approaching the dynamo onset the drop thus reduces. This rapid change of Ω marks the transition between the linear phase and the nonlinear phase. The saturated regime is characterized by strong fluctuations in both energies and enstrophy. Note in figure 1 (right) that the normalized cross helicity h_C starts to fluctuate in the nonlinear phase, showing a tendency towards an alignment of the $\boldsymbol{u}$ and $\boldsymbol{B}$ fields. We find $\left\langle h_C^2 \right\rangle^{1/2} = 0.03$ during the kinematic phase and $\left\langle h_C^2 \right\rangle^{1/2} = 0.23$ during the saturated phase. This alignment leads to a less efficient global electromotive force $\mathbf{u} \times \mathbf{b}$. In the sequel we will present another quantity whose statistics strongly changes from one regime to another and which allows for a more precise definition of the different phases of dynamo action. This quantity is in fact used to plot the vertical dashed lines in figure 1.

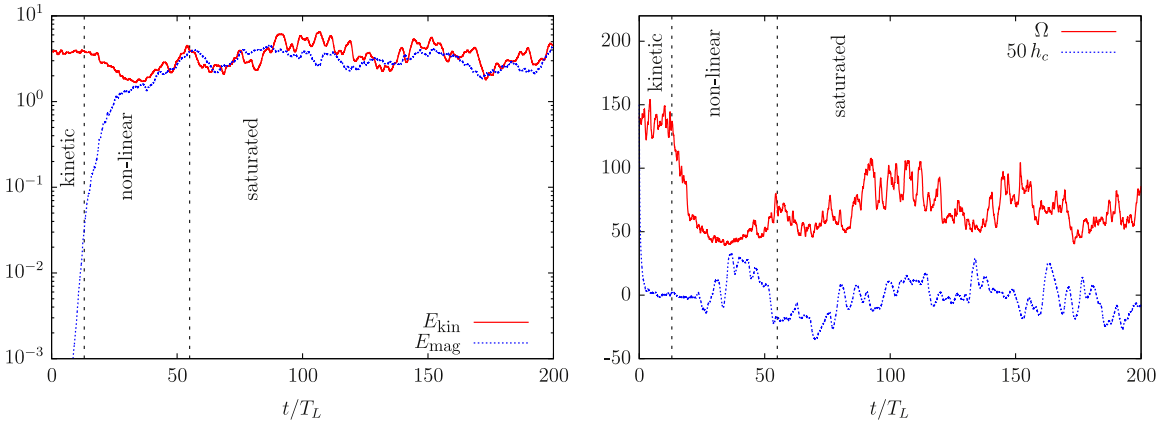

Figure 1. Temporal evolution of kinetic and magnetic energy (left). In the right panel the enstrophy and normalized cross helicity are shown. (all data for run tg3) The vertical dashed lines, representing the transition between the different phases have been determined by using the flatness of the magnetic field (see section 4 and figure 4). T_L is the large-eddy turn over-time measured at the saturated regime.

As mentioned before, the TG flow presents a manifest anisotropy coming from the very definition of the forcing. In the hydrodynamic regime we find a global isotropy coefficient $\rho_u^{\rm iso} = 0.74$ (see table 2). Anisotropy is even enhanced to $\rho_u^{\rm iso} \approx 0.36$ in the saturation regime, where large scale magnetic coherent structures appear in the two shear vortex plans and large tubes of kinetic energy are along the diagonal direction (see figure 2). We note that for the frozen force dynamo $\rho_u^{\rm iso}$ is close to unity during all phases of the simulation.

We now turn to the geometry of tracer trajectories. The linear phase is characterized by chaotic trajectories showing spiral motions around vorticity filaments (see figure 2 (top left)) which resemble trajectories in homogeneous and isotropic turbulence. The flow is approximately homogeneous.

In the saturated phase the flow structure and the geometry of the trajectories change (see top right panel of figure 2 and the supplementary movies available from stacks.iop.org/njp/16/075014/mmedia. One easily observes two manifestations of the smoothing effect of the magnetic field. First, vorticity filaments of the kinematic phase are quenched to vortex sheets in the saturated phase (see insets). Second, trajectories become highly aligned with the structures of the mean (time-averaged) kinetic and magnetic energy. These large-scale structures, well known in the literature, interconnect the fundamental boxes of the TG flow. In the vicinity of the diagonally oriented high kinetic energy tubes one observes streams of tracers with high velocities. They are separated by regions of chaotic motion (see figure 2 (bottom left)) which coincide with regions of low mean magnetic energy. From the bottom right panel of figure 2 one sees that perpendicular to the diagonal structures, the motion of tracer remains almost isotropic. For the frozen force (run ff), there is no large scale structure traversing the fundamental box (not shown). Blobs of increased magnetic energy are randomly distributed all over the cube. Tracer trajectories are in this case statistically homogeneous and isotropic.

4. Eulerian statistics

A turbulent flow naturally leads to magnetic field fluctuations which originate from stretching, twisting and diffusion of magnetic field lines. Under dynamo action the statistical properties of

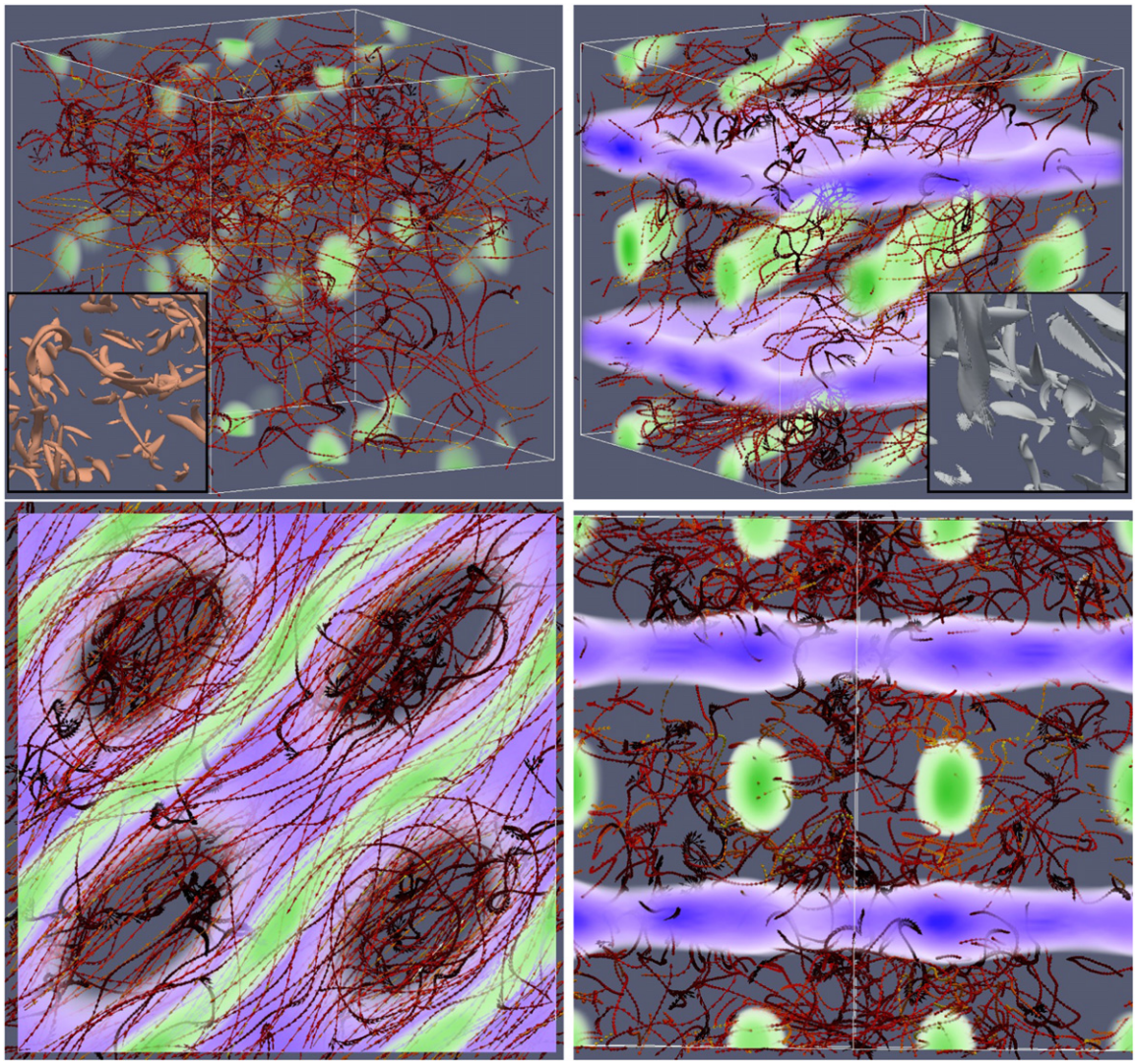

Figure 2. Volume rendering of the time-averaged kinetic energy (green) and magnetic energy (blue) for run tg3 together with tracer trajectories. Their speed is given in colors from black (low) to yellow (high). Left top: linear phase. The inset shows a snapshot of the enstrophy, where vortex filaments can be observed. Right top: saturated phase. The inset shows a snapshot of the enstrophy, where MHD vortex filaments and sheets are visible. Left bottom: top view (along z-axis) of the saturated phase. Right bottom: transverse view (along x,y-diagonal) of the saturated phase.

these fluctuations change significantly from one regime to another. In the linear phase, the probability density functions (PDFs) of the perpendicular magnetic field components present fat tails, far away from the Gaussian distribution (figure 3 (left)). Even at moderate Reynolds numbers we observe fluctuations of the magnetic field which are 15 times larger than its root mean square value. We emphasize that this non-Gaussian character of the magnetic field during the linear phase is also observed for the frozen large scale forcing (run ffH), as apparent in figure 3 (left). It has also been observed with a model using the recent fluid deformation closure [41]. This strongly suggests that the non-Gaussianity of the growing magnetic field is a generic

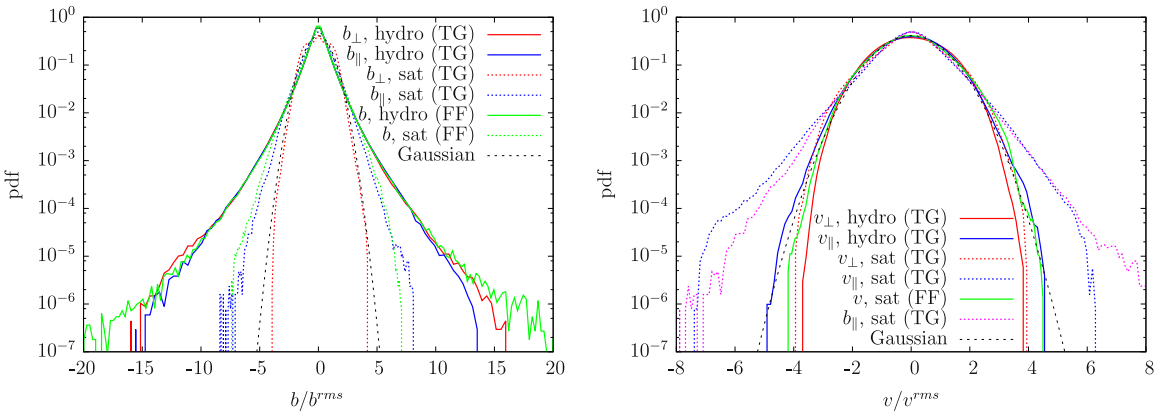

Figure 3. Probability distribution function of the magnetic field (left) and the velocity field (right) where the magnetic field component $b_\parallel$, *sat* (TG) is added for comparison. The data of the saturated Taylor–Green regime is from run tg3.

property of the linear phase. In contrast, the velocity field has nearly Gaussian statistics (see figure 3 (right)) as usually observed in hydrodynamic turbulence.

When the flow enters the saturated phase the normalized PDFs of the velocity and magnetic field components become similar. The tails of the perpendicular component $b_\perp$ of the magnetic field PDF shrink to quasi-Gaussian tails (figure 3 (left)). The perpendicular component of the velocity field $v_\perp$ remains Gaussian. Such magnetic-field PDFs along the saturated regime have also been observed in the VKS experiment [4]. The parallel component of the velocity field seems to follow the magnetic field: the PDF of $b_\parallel$ remains non-Gaussian and that of $v_\parallel$ develops non-Gaussian tails. A reason for this matching of velocity and magnetic field PDFs might be the increased alignment of v and b in the saturated regime (indicated by the increase of h_c in figure 1) which couples kinetic and magnetic fluctuations. Also in recent models of the energy spectrum of MHD turbulence a scale dependent alignment plays an important role [42].

In order to estimate the non-Gaussianity of a field f, the temporal evolution of its flatness $\langle f^4 \rangle / \langle f^2 \rangle^2$ is measured. The flatness of the magnetic field starts from a large value (see figure 4) originating from their stretched tails. During the nonlinear phase its flatness strongly reduces and reaches a slightly sub-Gaussian value for the perpendicular component $b_\perp$ while it is super-Gaussian for the parallel component $b_\parallel$. A significant change can also be observed for the flatness of the velocity field PDFs (see also figure 4). The perpendicular component $v_\perp$ starts slightly sub-Gaussian and fluctuates around the Gaussian value 3, while the flatness of the component $v_\parallel$ is clearly larger and comparable to that of $b_\parallel$ during the saturated phase. These changes in the behavior of the flatness temporal evolution allow to clearly distinguish the three phases of the dynamo action indicated by the vertical lines drawn in figures 1 and 4.

We now turn to the statistics of a small scale quantity of the flow, namely the fluid acceleration, whose PDFs are displayed in figure 5 (left). Contrarily to the PDFs of the velocity, a large scale quantity, there are no significant differences among perpendicular and parallel components. This is in agreement with the general observation that isotropy is recovered at small scales in turbulent flows. In order to improve statistics, the three acceleration components have been averaged. The acceleration has strongly non-Gaussian tails, as usually observed in

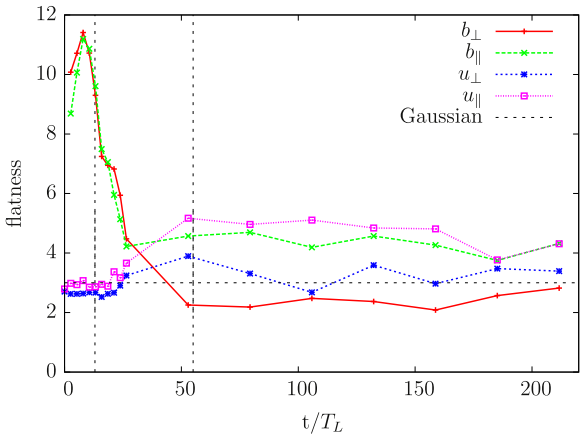

Figure 4. Temporal evolution of the flatness of the magnetic and velocity field PDFs for run tg3. T_L is the large-eddy turn over-time measured at the saturated regime.

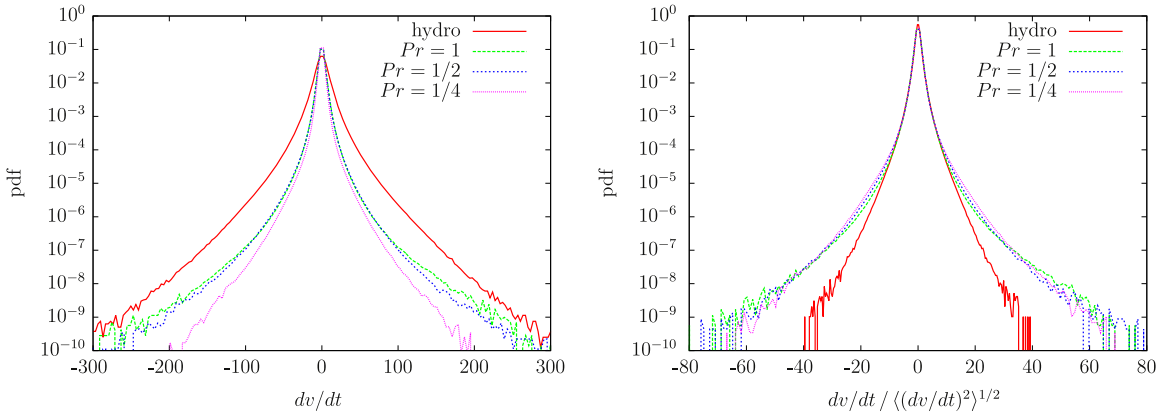

Figure 5. Probability distribution function of acceleration. Non-normalized (left) and normalized to standard deviation (right) for a hydrodynamic simulation (run tgH) and saturated regimes (run tg1, tg2 and tg3).

turbulent flows, [23] and decreases from the kinematic to the saturated phase (see figure 5 (left)). This is in consistent with the known fact that the saturation regime smoothes out the small scales of the velocity. Indeed, the rms acceleration reduces from $a_{\rm rms} = 80$ for the hydrodynamic phase to $a_{\rm rms} = 16$ and $a_{\rm rms} = 10$ for the saturated phase for $Pm = 1$ and $Pm = 1/4$, respectively. Smaller magnetic Prandtl numbers thus imply smaller accelerations. However, when comparing the normalized PDFs (normalized to standard deviation, figure 5 (right)), the Prandtl number has only a negligible effect. The PDFs for different Pm fall roughly on top of each other but clearly have fatter tails than the PDF of the kinematic regime. This means that the dynamics of a saturated dynamo leads to significantly more extreme accelerations events than in pure hydrodynamics. The flatness of the PDFs reaches 25 in the saturated regime, while it is 14 in the hydro case.

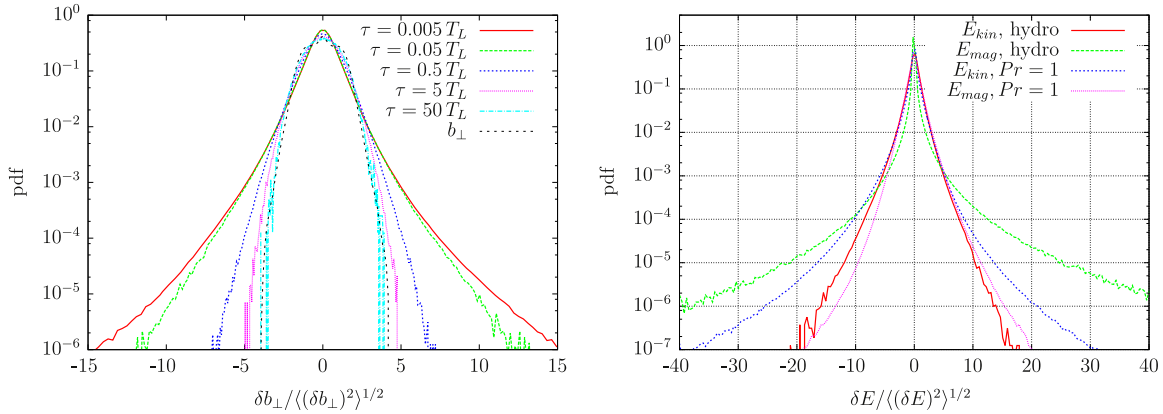

Figure 6. Left: PDFs of the magnetic field increments in the perpendicular direction along fluid element trajectories for several time lags in the saturated phase. For comparison the PDF of the $b_\perp$ is shown. (data from run tg3) Right: PDFs of the magnetic field energy increments for τ of the order of $5 \times 10^{-3} T_L \sim \tau_K$.

5. Lagrangian statistics

5.1. Magnetic and energy increments

We now turn to study the properties of the magnetic field along fluid element trajectories, i.e. the magnetic field seen by a tracer. We will first focus on changes in the perpendicular component of the magnetic field, the dominant component of the mean field. For this, we consider the temporal increment $\delta b_\perp(\tau, t, \boldsymbol{x}) = B_\perp(\boldsymbol{X}(\boldsymbol{x}, t+\tau), t+\tau) - B_\perp(\boldsymbol{X}(\boldsymbol{x}, t), t)$ where $B_\perp$ denotes a magnetic field component from the perpendicular plane (B_x or B_y) and $\boldsymbol{X}(\boldsymbol{x}, t)$ a fluid trajectory starting at $\boldsymbol{x}$ at a time t. τ denotes the time lag between two points of a tracer trajectory. To improve statistics we average over $\boldsymbol{x}$ and t which leads to the study of the magnetic field increment

$$\delta b_\perp(\tau) = b_\perp(\tau) - b_\perp(0). \tag{7}$$

The normalized PDFs of the increment $\delta b_\perp$ during the saturated phase are shown in figure 6 (left) for different time lags. On short time scales the PDFs are strongly non-Gaussian. Stretched tails have been also observed for small scale magnetic fluctuations in the solar wind [43]. For time lags the PDF becomes Gaussian. This is simply due to the time decorrelation of $b_\perp(\tau)$ and $b_\perp(0)$ so that one recovers for large τ the one-point Gaussian Eulerian PDF shown in figure 3 (left). It is important to stress that the time scale τ at which this decorrelation takes place is unusually long. It exceeds significantly one large-eddy turn-over time. The associated long time regime will be analyzed in detail in the next subsection.

Finally, we investigate how the Lorentz force modifies the Lagrangian kinetic energy increments

$$\delta E_v(\tau) = \frac{1}{2}\Big(\boldsymbol{v}^2(\tau) - \boldsymbol{v}^2(0)\Big). \tag{8}$$

This quantity has recently attracted interest [44] because it allows to characterize the irreversibility of turbulent flows. In figure 6 we plot PDFs of δE_v and also those of the magnetic

energy δE_m for the kinematic and saturated regime. They are non-Gaussian and not symmetric unlike $\delta b_\perp$. A measure of their asymmetry is the skewness $S_f = \left\langle f^3 \right\rangle / \left\langle f^2 \right\rangle^{3/2}$. For the hydro case the PDF of the kinetic energy has a negative skewness of $S_v \approx -0.4$ which is close to the value reported in [44]. We note that the Lagrangian derivative $d|\boldsymbol{u}|^2/\mathrm{d}t$ can be written in terms of Eulerian quantities $d|\boldsymbol{u}|^2/\mathrm{d}t = 2\left(|\boldsymbol{u}|^2 \nabla_{\boldsymbol{u}}^{\parallel} \boldsymbol{u} + \boldsymbol{u}\partial_t \boldsymbol{u}\right)$, where $\nabla_{\boldsymbol{u}}^{\parallel}\boldsymbol{u}$ is the longitudinal velocity gradient $\nabla_r^{\parallel}\boldsymbol{u} \equiv \hat{\boldsymbol{r}} \cdot \left(\hat{\boldsymbol{r}} \cdot \nabla \boldsymbol{u}\right)$ evaluated in the direction of the local velocity $\hat{\boldsymbol{u}}$. As for small time lags $\delta E_v(\tau) \sim \tau d|\boldsymbol{u}|^2/\mathrm{d}t$, the asymmetry of the red curve in figure 6 (right) may be a consequence of the skewness of $\nabla_r^{\parallel}\boldsymbol{u}$ reported in the literature [46].

A negative skewness means that violent decelerations are more probable than violent accelerations. The skewness of the velocity PDFs decreases towards the saturated regime ($S_v \approx -1.0$ for $Pm = 1/4$, $S_v \approx -1.2$ for $Pm = 1/2$ and $S_v \approx -1.2$ for $Pm = 1$). In contrast, the magnetic field PDF has a positive skewness $S_b \approx 2.5$ during the kinematic phase, which decreases in the saturated phase ($S_b \approx 0.43$ for $Pm = 1/4$, $S_b \approx 0.32$ for $Pm = 1/2$ and $S_b \approx 0.34$ for $Pm = 1$). The change of the skewness between the different phases is certainly related to the nonlinear exchange between the kinetic and the magnetic energies, which are local and non-local in a large range of scale [45].

5.2. Long time correlations

In the previous section we observed that the transition to Gaussian statistics of the perpendicular magnetic field takes very long times during the saturated regime while in the kinematic regime this happens on time scales of the order of T_L. The reason are long lasting correlations. The autocorrelation of the Lagrangian velocity $C_v(\tau) = \left\langle v_i'(t)\, v_i'(t+\tau) \right\rangle / \left\langle v_i'^2(t) \right\rangle$ with $v_i'(t) = v_i(t) - \left\langle v_i(t) \right\rangle$, is displayed in figure 7 (left). The Lagrangian correlation time is indeed of the order T_L for the hydrodynamic regime. During the saturated regime the perpendicular component of the velocity field remains correlated for a longer time (see figure 7 (left)) of the order of several T_L. Note that the parallel component becomes anti-correlated at times of the order of π/v_z^{rms} (see table 2). This corresponds to the typical time of a fluid particle crossing a TG fundamental box in the z direction and starting to feel the mirror symmetries of the TG flow.

The long correlation time scale is also clearly observed for the magnetic field in figure 7 (right) and corresponds to the time-lag for which the PDF of the magnetic field increments becomes Gaussian. We note that this time scale is a specific property of the TG flow which is not observed with the frozen force (run ff, figure 6 (right)) and it only weakly depends on Pm (not shown).

In order to better understand the long time correlations and the non-Gaussianity of the magnetic field increments we study Lagrangian structure functions (LSF) of the form

$$S_p^B(\tau) = \left\langle \left| B_\perp(t+\tau) - B_\perp(t) \right|^p \right\rangle, \tag{9}$$

during the saturated phase. Here again, $B_\perp$ denotes a magnetic field component from the perpendicular plane (B_x or B_y). In turbulent flows the structure functions are usually measured to identify and to analyze the scales of the inertial range (for u_i instead of B_i) in which they behave as a power law $S_p(\tau) \sim \tau_p^\zeta$. The corresponding scaling exponents ζ_p provide a handle on the

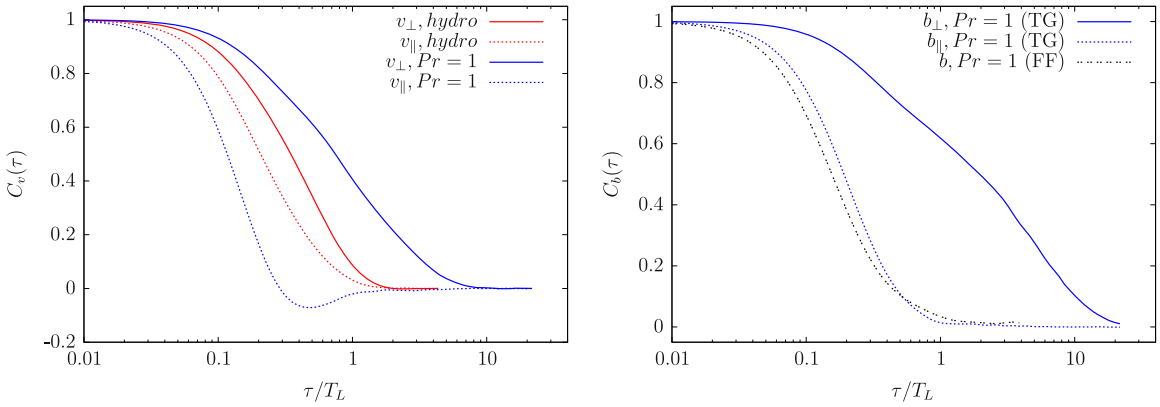

Figure 7. Left: autocorrelation functions $C_v(\tau)$ of the velocity along trajectories in the hydrodynamic phase (run tgH) and saturated phase (run tg3). Right: autocorrelation functions $C_b(\tau)$ of the magnetic field measured along trajectories for the saturated phase for run tg3, and ff. T_L is the large-eddy turn over-time measured at the saturated regime.

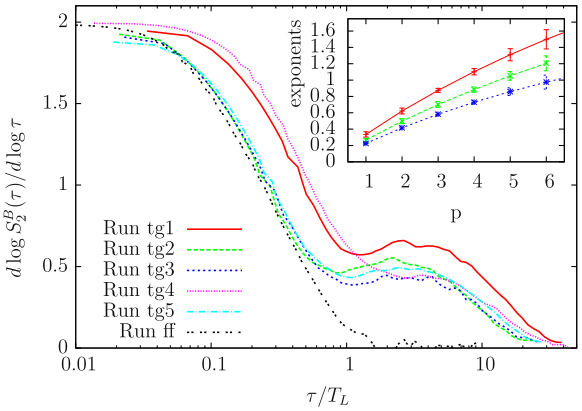

Figure 8. Local slope of the second order Lagrangian structure functions of the magnetic field $S_2^B(\tau)$ for all runs in the saturated regime. The inset shows the measured scaling exponents ζ_p^B different orders p. Error bars give the maximal variation around the mean in the interval where S_2^B is flat. (data from run tg1, tg2 and tg3) T_L is the large-eddy turn over-time measured at the saturated regime.

phenomenon of intermittency which characterizes the occurrence of extreme events in the dynamical evolution of the system [46]. A scaling range and the corresponding scaling exponents can reliably be measured via the local slope of the structure functions that is their logarithmic derivative $d \log S_p / d \log \tau$. This quantity for the second order LSF S_2^B is shown in figure 8 for all runs. In hydrodynamic turbulence, even for very large Reynolds numbers, the range of temporal scales where a power law is observed and where thus the local slope is constant is very narrow if visible at all [47]. We therefore do not expect to observe a power-law behavior on time-scales shorter than 1 T_L. Surprisingly, for larger times scales a clear plateau is apparent for the TG runs. Its width is similar (from approximately 1 T_L to 10 T_L) for all runs but run tg4 (forced at $k_0 = 2$) indicating a relationship with the scale of the forcing. The

corresponding scaling exponent does not seem to depend on the Reynolds number of the flow while it changes depending on the magnetic Prandtl number: it decreases when increasing *Pm*. As expected, for the frozen-force simulation (ff) where correlations do not persist beyond 1 T_L, no scaling region is observed.

Higher order statistics reveals that the magnetic fluctuations in this scaling region are intermittent. The scaling exponents ζ_p^B of the structure functions S_p^B are shown in the inset of figure 8 for three different Prandtl numbers. They reveal that the long time magnetic fluctuations are intermittent as all curves are bent. Concerning their magnetic Prandtl number dependence one finds that the values of the exponents grow when decreasing *Pm* but we note that the curves of the relative scaling exponents ζ_p/ζ_2 fall on top of each other within the error bars (not shown).

In order to better understand the origin of the observed long time correlations we computed the energy sources and sinks of the velocity field. We find that the correlation time of the mean external energy injection rate $\langle \boldsymbol{u} \cdot \boldsymbol{F} \rangle$ becomes longer during the nonlinear phase and extends well beyond 1 T_L during the saturated phase. The total energy of the system also fluctuates on this time scale. This is in agreement with the observed changes of the correlation time of $u_\perp$ in figure 7 (left) as the TG force is constant. The energy exchange time scale $\langle \boldsymbol{u} \cdot (\nabla \times \boldsymbol{B}) \times \boldsymbol{B} \rangle$ connected to the Lorentz force is shorter. We note that the mean external energy injection rate is a large-scale quantity. Apparently, the Lorentz force changes the global flow structure in such a way that the resulting large-scale velocity field and the (constant) TG force remain correlated for times much longer than without Lorentz force. The observed scaling regime is probably not a classical turbulent scaling regime.

We complement the discussion of the long time scaling regime by analyzing the power density spectrum (PDS) of the perpendicular magnetic field $b_\perp$ along tracer trajectories. For the PDS we find a low frequency band showing a power-law decay (see figure 9 (left)). The slope ζ_2 of a second order structure function and that of the corresponding PDS (α) are connected via the formula $\alpha = -\zeta_2 - 1$ [46]. The measured slopes of the PDS are consistent with the scaling exponents of the structure functions.

Finally, we note that the slopes of the spectra of $b_\perp$ are also compatible with the slopes of the spectra of the total magnetic energy $E_{\mathrm{mag}}(t)$ (see figure 9 (right)). Keeping in mind that the PDS of $E_{\mathrm{mag}}(t)$ has a dimension B^2 and the PDS of $b_\perp$ a dimension of B one finds an agreement by simple dimensional analysis.

6. Conclusions

By means of direct numerical simulations of the MHD equations forced by the TG vortex we analyzed Lagrangian statistics during the three stages of a dynamo system: the kinematic phase, the nonlinear phase and the saturated phase.

The Lagrangian view point reveals substantial changes in the dynamics between the kinematic phase and saturated phase. On the one hand the magnetic field produced by dynamo action smoothes the flow: fluid accelerations reduce on average and tracer trajectories change from quasi-chaotic to highly mean magnetic field aligned. During its exponential growth, the created magnetic field is highly non-Gaussian while it becomes quasi-Gaussian during

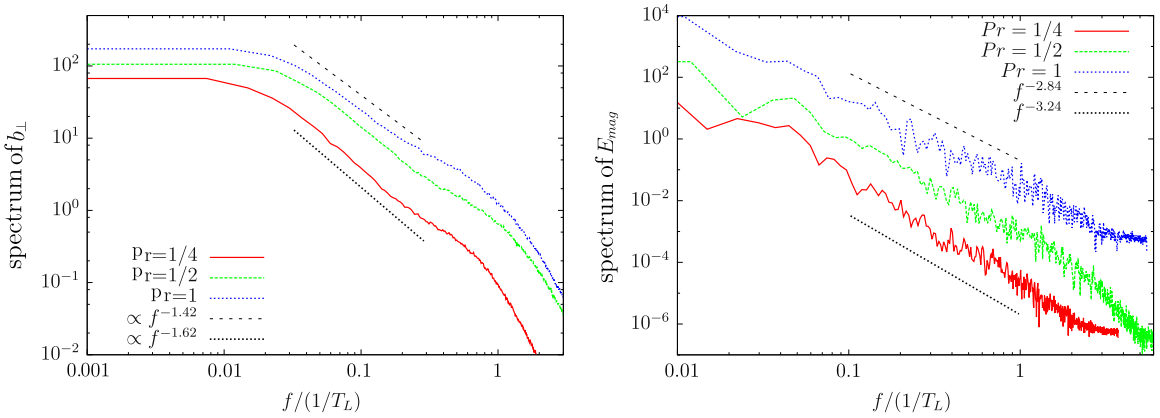

Figure 9. Left: power density spectrum (PDS) of $b_\perp$ for run tg1, tg2, and tg3. The frequency f is given in terms of the large scale frequency $1/T_L$. Right: PDS of the total magnetic energy $E_{\rm mag}\,(t)$ for run tg1, tg2 and tg3. All curves are shifted for clarity. T_L is the large-eddy turn-over time measured at the saturated regime.

saturation. On the other hand the fluid experiences more violent acceleration events in the saturated phase than in the kinematic phase. Temporal correlations extend much longer in the saturated regime than in the kinematic one, exceeding significantly usual turbulent time scales.

At time scales approximately ranging from one to ten large-eddy turn-over times we find a clear scaling regime of magnetic field increments along particle trajectories. High-order scaling exponents of the LSF show that these long-time magnetic field fluctuations are intermittent and that intermittency is increasing with increasing magnetic Prandtl number. The second-order scaling is consistent with a power-law observed for the corresponding frequency spectrum and that of fluctuations of the total magnetic energy of the system.

Additionally, we find that the PDFs of magnetic and velocity energy increments along tracer trajectories are skewed. We find a positive skewness for the magnetic energy which reduces from the kinematic to the saturated phase. The skewness of the kinetic energy is negative during the kinematic phase and is even smaller during the saturated phase. The evolution of the skewness of PDF energy increment is clearly due the energy transfer between the kinetic and magnetic energies.

Finally, we would like to mention that we do not observe a long time scaling regime for simulations with an ABC force. If this scaling regime is specific to the TG force or if other forces lead to similar long time dynamics has to be investigated in future work.

Acknowledgments

We thank J F Pinton for useful discussions. Access to the IBM BlueGene/P computer JUGENE at the FZ Jülich was made available through project HBO22 and partly through project HBO36. Computer time was also provided by GENCI and the Mesocentre SIGAMM machine. This work benefited from support through DFG-FOR1048.

References

[1] Gailitis A, Lielausis O, Dement'ev S, Cifersons A, Gerbeth G, Gundrum T, Christen F S M, Anel H H and Will G 2001 Magnetic field saturation in the Riga dynamo experiment *Phys. Rev. Lett.* **86** 3024

[2] Stieglitz R and Müller U 2001 Experimental demonstration of a homogeneous two-scale dynamo *Phys. Fluids* **13** 561

[3] Monchaux R *et al* 2007 Generation of a magnetic field by dynamo action in a turbulent flow of liquid sodium *Phys. Rev. Lett.* **98** 044502

[4] Monchaux R *et al* 2009 The von Kármán Sodium experiment: turbulent dynamical dynamos *Phys. Fluids* **21** 035108

[5] Berhanu M *et al* 2010 Dynamo regimes and transitions in the VKS experiment *Eur. Phys. J.* B **77** 459–68

[6] Gallet B *et al* 2012 Experimental observation of spatially localized dynamo magnetic fields *Phys. Rev. Lett.* **108** 144501

[7] Childress S and Gilbert A 1995 *Stretch, Twist, Fold: The Fast Dynamo* (Berlin: Springer)

[8] Ponty Y, Minnini P, Pinton J-F, Politano H and Pouquet A 2007 Dynamo action at low magnetic Prandtl numbers: mean flow versus fully turbulent motions *New J. Phys.* **9** 296

[9] Ponty Y and Plunian F 2011 Transition from large-scale to small-scale dynamo *Phys. Rev. Lett.* **106** 154502

[10] Dubrulle B, Blaineau P, Mafra O L, Daviaud F, Laval J and Dolganov R 2007 Bifurcations and dynamo action in a Taylor–Green flow *New J. Phys.* **9** 308

[11] Schekochihin A A, Iskakov A B, Cowley S C, McWilliams J C, Proctor M R E and Yousef T A 2007 Fluctuation dynamo and turbulent induction at low magnetic Prandtl numbers *New J. Phys.* **9** 300

[12] Cattaneo F, Hughes D and Kim E 1996 Suppression of chaos in a simplied nonlinear dynamo model *Phys. Rev. Lett.* **76** 2057–60

[13] Zienicke E, Politano H and Pouquet A 1998 Variable intensity of Lagrangian chaos in the nonlinear dynamo problem *Phys. Rev. Lett.* **81** 4640–4640

[14] Pinton J and Ponty Y 2007 private communication *Roma airport back from a conference in Catania*

[15] Toschi F and Bodenschatz E 2009 Lagrangian properties of particles in turbulence *Ann. Rev. Fluid Mech.* **41** 375–404

[16] Biferale L, Boffetta G, Celani A, Devenish B J, Lanotte A and Toschi F 2004 Multifractal statistics of Lagrangian velocity and acceleration in turbulence *Phys. Rev. Lett.* **93** 4502

[17] Yeung P K and Sawford M S 2006 Reynolds number dependence of Lagrangian statistics in large numerical simulations of isotropic turbulence *J. Turbulence* **7** 1–12

[18] Bec J, Biferale L, Boffetta G, Celani A, Cencini M, Lanotte A, Musaccio S and Toschi F 2006 Acceleration statistics of heavy particles in turbulence *J. Fluid Mech.* **550** 349–58

[19] Yeung P K and Borgas M S 2004 Relative dispersion in isotropic turbulence: Part 1. Direct numerical simulations and Reynolds-number dependence *J. Fluid Mech.* **503** 93–124

[20] Homann H, Bec J, Fichtner H and Grauer R 2009 Clustering of passive impurities in MHD turbulence *Phys. Plasma* **16** 082308

[21] Eyink G, Vishniac E, Lalescu C, Aluie H, Kanov K, Bürger K, Burns R, Meneveau C and Szalay A 2013 Flux-freezing breakdown in high-conductivity magnetohydrodynamic turbulence *Nature* **497** 466–9

[22] Mordant N, Delour J, Léveque E, Arnéodo A and Pinton J-F 2002 Long time correlations in Lagrangian dynamics: a key to intermittency in turbulence *Phys. Rev. Lett.* **89** 254502

[23] La Porta A, Voth G A, Crawford A M, Alexander J and Bodenschatz E 2001 Fluid particle accelerations in fully developed turbulence *Nature* **409** 1017–9

[24] Homann H, Grauer R, Busse A and Müller W C 2007 Lagrangian statistics of Navier–Stokes and MHD turbulence *J. Plasma Phys.* **73** 821–30

[25] Homann H, Kamps O, Friedrich R and Grauer R 2009 Bridging from Eulerian to Lagrangian statistics in 3d hydro and magnetohydrodynamic turbulent flows *New J. Phys.* **11** 073020

[26] Celani A, Mazzino A and Vincenzi D 2006 Magnetic field transport and kinematic dynamo effect: a Lagrangian interpretation *Proc. R. Soc.* A **462** 137–47
[27] Brachet M E, Meiron D I, Orszag S A, Nickel B G, Morf R H and Frisch U 1983 Small-scale structure of the Taylor–Green vortex *J. Fluid Mech.* **130** 411–52
[28] Nore C, Brachet M, Politano H and Pouquet A 1997 Dynamo action in the Taylor–Green vortex near threshold *Phys. Plasmas* **4** 1
[29] Ponty Y, Pouquet P M A, Politano H, Montgomery D and Pinton J 2005 Numerical study of dynamo action at low magnetic Prandtl numbers *Phys. Rev. Lett.* **94** 164512
[30] Mininni P D, Ponty Y, Montgomery D C, Politano J-F P H and Pouquet A 2005 Dynamo regimes with a non-helical forcing *Astrophys. J.* **626** 853–63
[31] Ponty Y, Mininni P D, Laval J-P, Alexakis A, Baerenzung J, Daviaud F, Dubrulle B, Pinton J-F, Politano H and Pouquet A 2008 Linear and non linear features of the Taylor–Green dynamo *C. R. Phys.* **9** 749–56
[32] Krstulovic G, Thorner G, Vest J-P, Fauve S and Brachet M 2011 Axial dipolar dynamo action in the Taylor–Green vortex *Phys. Rev.* E **84** 066318
[33] Dijkstra D and Heijst G J F V 1983 The flow between two finite rotating disks enclosed by a cylinder *J. Fluid Mech.* **128** 123–54
[34] Fauve S, Laroche C and Castaing B 1993 Pressure fluctuations in swirling turbulent flows *J. Phys.* II **3** 271–8
[35] Labbé R, Pinton J-F and Fauve S 1996 Study of the von Kàrmàn flow between coaxial corotating disks *Phys. Fluids* **8** 914–22
[36] Cadot O, Couder Y, Daerr A, Douady S and Tsinober A 1997 Energy injection in closed turbulent flows: stirring through boundary layers versus inertial stirring *Phys. Rev.* E **56** 427
[37] de la Torre A and Burguete J 2007 Slow dynamics in a turbulent von Kàrmàn swirling flow *Phys. Rev. Lett.* **99** 054101–4
[38] Ravelet F, Marié L, Chiffaudel A and Daviaud F c 2004 Multistability and memory effect in a highly turbulent flow: experimental evidence for a global bifurcation *Phys. Rev. Lett.* **93** 164501
[39] Ravelet F, Chiffaudel A and Daviaud F 2008 Supercritical transition to turbulence in an inertially driven von Kármán closed flow *J. Fluid Mech.* **601** 339–64
[40] Homann H, Dreher J and Grauer R 2007 Impact of the floating-point precision and interpolation scheme on the results of DNS of turbulence by pseudo-spectral codes *Comput. Phys. Commun.* **177** 560–5
[41] Hater T, Homann H and Grauer R 2011 Lagrangian model for the evolution of turbulent magnetic and passive scalar fields *Phys. Rev.* E **83** 017302
[42] Boldyrev S 2006 Spectrum of magnetohydrodynamic turbulence *Phys. Rev. Lett.* **96** 115002
[43] Alexandrova O, Carbone V, Veltri P and Sorriso-Valvo L 2008 Small-scale energy cascade of the solar wind turbulence *Astrophys. J.* **674** 1153
[44] Xu H, Pumir A, Falkovich G, Bodenschatz E, Shats M, Xia H, Francois N and Boffetta G 2013 Power fluctuations and irreversibility in turbulence arXiv:1310.5006
[45] Alexakis A, Mininni P D and Pouquet A 2005 Shell-to-shell energy transfer in magnetohydrodynamics. I. steady state turbulence *Phys. Rev.* E **72** 046301
[46] Frisch U 1955 *Turbulence* (Cambridge: Cambridge University Press)
[47] Falkovich G, Xu H, Pumir A, Bodenschatz E, Biferale L, Boffetta G, Lanotte A and Toschi F 2012 On Lagrangian single-particle statistics *Phys. Fluids* **24** 055102